Journal Pre-proof

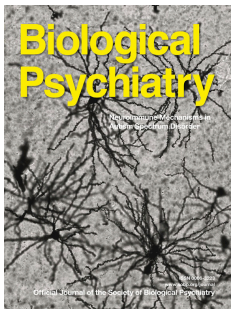

Signature of altered retinal microstructures and electrophysiology in schizophrenia spectrum disorders is associated with disease severity and polygenic risk

Emanuel Boudriot, Vanessa Gabriel, David Popovic, Pauline Pingen, Vladislav Yakimov, Sergi Papiol, Lukas Roell, Genc Hasanaj, Simiao Xu, Joanna Moussiopoulou, Siegfried Priglinger, Christoph Kern, Eva C. Schulte, Alkomiet Hasan, Oliver Pogarell, Peter Falkai, Andrea Schmitt, Benedikt Schworm, CDP Working Group, Elias Wagner, Daniel Keeser, Florian J. Raabe

PII: S0006-3223(24)01262-9

DOI: https://doi.org/10.1016/j.biopsych.2024.04.014

Reference: BPS 15478

To appear in: *Biological Psychiatry*

Received Date: 3 August 2023

Revised Date: 30 March 2024

Accepted Date: 14 April 2024

Please cite this article as: Boudriot E., Gabriel V., Popovic D., Pingen P., Yakimov V., Papiol S., Roell L., Hasanaj G., Xu S., Moussiopoulou J., Priglinger S., Kern C., Schulte E.C., Hasan A., Pogarell O., Falkai P., Schmitt A., Schworm B., CDP Working Group , ,, Wagner E., Keeser D. & Raabe F.J., Signature of altered retinal microstructures and electrophysiology in schizophrenia spectrum disorders is associated with disease severity and polygenic risk, *Biological Psychiatry* (2024), doi: https://doi.org/10.1016/j.biopsych.2024.04.014.

Signature of altered retinal microstructures and electrophysiology in schizophrenia spectrum disorders is associated with disease severity and polygenic risk

Emanuel Boudriot[1,2,*] (ORCID iD: 0000-0001-6083-6318), Vanessa Gabriel[1,*], David Popovic[1,2] (ORCID iD: 0000-0002-2367-9437), Pauline Pingen[1], Vladislav Yakimov[1,3] (ORCID-iD: 0000-0001-9559-7492), Sergi Papiol[2,4] (ORCID iD: 0000-0001-9366-8728), Lukas Roell[1,5] (ORCID iD: 0000-0002-0284-2290), Genc Hasanaj[1,6], Simiao Xu[1], Joanna Moussiopoulou[1] (ORCID iD: 0000-0002-0157-6197), Siegfried Priglinger[7], Christoph Kern[7], Eva C. Schulte[4,8,9] (ORCID iD: 0000-0003-3105-5672), Alkomiet Hasan[10,11], Oliver Pogarell[1], Peter Falkai[1,2,11] (ORCID iD: 0000-0003-2873-8667), Andrea Schmitt[1,2,11] (ORCID iD 0000-0002-5426-4023), Benedikt Schworm[7], CDP Working Group[1,2,6,10], Elias Wagner[6,10], Daniel Keeser[1,5,13] (ORCID iD: 0000-0002-0244-1024), Florian J. Raabe[1,2,#] (ORCID iD: 0000-0001-8538-0783)

[1]Department of Psychiatry and Psychotherapy, LMU University Hospital, LMU Munich, 80336 Munich, Germany

[2]Max Planck Institute of Psychiatry, 80804 Munich, Germany

[3]International Max Planck Research School for Translational Psychiatry (IMPRS-TP), 80804 Munich, Germany

[4]Institute of Psychiatric Phenomics and Genomics, LMU Munich, 80336 Munich, Germany

[5]NeuroImaging Core Unit Munich (NICUM), LMU University Hospital, LMU Munich, 80336 Munich, Germany

[6]Evidence-based psychiatry and psychotherapy, Faculty of Medicine, University of Augsburg, 86156 Augsburg, Germany

[7]Department of Ophthalmology, LMU University Hospital, LMU Munich, 80336 Munich, Germany

[8]Institute of Human Genetics, University Hospital, Faculty of Medicine, University of Bonn, 53127 Bonn, Germany

[9]Department of Psychiatry and Psychotherapy, University Hospital, Faculty of Medicine, University of Bonn, 53127 Bonn, Germany

[10]Department of Psychiatry, Psychotherapy, and Psychosomatics, Faculty of Medicine, University of Augsburg, 86156 Augsburg, Germany

[11]German Center for Mental Health (DZPG), partner site Munich-Augsburg

[12]Laboratory of Neurosciences (LIM-27), Institute of Psychiatry, University of São Paulo (USP), São Paulo-SP 05403-903, Brazil

[13]Munich Center for Neurosciences (MCN), LMU Munich, 82152 Planegg-Martinsried, Germany

*These authors contributed equally.

#Corresponding author: Florian J. Raabe, MD, PhD; Department of Psychiatry and Psychotherapy, LMU University Hospital, LMU Munich, Nußbaumstraße 7, 80336 Munich, Germany; e-mail: florian.raabe@med.uni-muenchen.de

Running title: Retinal alterations in schizophrenia spectrum disorders

Keywords (max. 6): optical coherence tomography (OCT), electroretinography (ERG), magnetic resonance imaging (MRI), schizophrenia, retina, genetics

Supplemental Information:

- Supplemental Document (PDF): 3 Supplemental Figures and Supplemental Methods
- 1 Excel File including 13 worksheets with 12 Supplemental Tables

Abstract

BACKGROUND: Optical coherence tomography (OCT) and electroretinography (ERG) studies have revealed structural and functional retinal alterations in individuals with schizophrenia spectrum disorders (SSD). However, it remains unclear which specific retinal layers are affected, how the retina, brain, and clinical symptomatology are connected, and how alterations of the visual system are related to genetic disease risk.

METHODS: OCT, ERG, and brain magnetic resonance imaging (MRI) were applied to comprehensively investigate the visual system in a cohort of 103 patients with SSD and 130 healthy control individuals. The sparse partial least squares (SPLS) algorithm was used to identify multivariate associations between clinical disease phenotype and biological alterations of the visual system. The association of the revealed patterns with the individual polygenetic disease risk for schizophrenia was explored in a post hoc analysis. In addition, covariate-adjusted case-control comparisons were performed for each individual OCT and ERG parameter.

RESULTS: The SPLS analysis yielded a phenotype-eye-brain signature of SSD in which greater disease severity, longer duration of illness, and impaired cognition were associated with electrophysiological alterations and microstructural thinning of most retinal layers. Higher individual loading onto this disease-relevant signature of the visual system was significantly associated with elevated polygenic risk for schizophrenia. In case-control comparisons, patients with SSD had lower macular thickness, thinner retinal nerve fiber and inner plexiform layers, less negative a-wave amplitude, and lower b-wave amplitude.

CONCLUSIONS: This study demonstrates multimodal microstructural and electrophysiological retinal alterations in individuals with SSD that are associated with disease severity and individual polygenetic burden.

Introduction

An increasing number of studies indicate retinal alterations in individuals with schizophrenia spectrum disorders (SSD) (1-3). Based on a common embryonic origin (4, 5), the retina shares numerous anatomical and physiological similarities with the brain (6, 7). Accordingly, it has been postulated that the retina is an easily accessible “window to the brain” (6, 8).

Unlike the brain, retinal structures can be studied noninvasively in much greater detail, at a resolution of a few micrometers, with the light-based method of optical coherence tomography (OCT; **Figure S1**) (9). Previous OCT studies in individuals with SSD provide strong evidence for reduced overall macular thickness (MT) and a thinner peripapillary retinal nerve fiber layer (RNFL) and ganglion cell–inner plexiform layer (GCIPL) compared to healthy controls (HC), which has also been confirmed in recent meta-analyses (1, 2, 10, 11). However, regarding the effect sizes on MT, RNFL, and GCIPL and alterations of other retinal layers, the results of previous studies contain some heterogeneity, possibly due to small sample sizes of many studies, varying sample compositions (e.g., chronic vs acute disease stages) as well as the heterogeneity of SSD themselves (2, 3, 11-20). Moreover, due to technical limitations of the applied OCT technology (21) and image segmentation procedures (22), most previous studies have focused only on the total retinal thickness and the thicknesses of the inner retinal layers (2). Meanwhile, advances in OCT technology, including the advent of spectral-domain OCT, have enabled reliable segmentation of all individual retinal layers (21). In SSD, so far only a few, low-powered studies with 25 to 35 patients and 15 to 50 HC have analyzed all retinal layers individually and also indicated alterations of the outer retinal layers, especially the outer nuclear layer (ONL) (23-26). Thus, larger studies are required to confirm which individual retinal layers are particularly affected in SSD.

Furthermore, recent studies have also indicated electrophysiological alterations of the outer retinal layers in SSD (3, 10, 27-34). A well-established tool to study retinal function is electroretinography (ERG; **Figure S1**), which measures the electrical response of retinal cells to light stimuli (28). Recent ERG studies in individuals with schizophrenia (SZ) pointed to a

dysfunction of photoreceptors and bipolar cells (27, 28, 31) that appeared to be, in part, independent of antipsychotic medication (27, 28).

Although there is also evidence for alterations of the visual cortex in psychotic disorders (35), little is known about the extent to which retinal and cerebral alterations in SSD are intertwined. Only few studies have integrated magnetic resonance imaging (MRI) and OCT data in SSD, suggesting co-impairment of the retina and visual cortex (36-39) as well as a possible link between ONL thinning and reduced total brain and white matter volumes in psychosis patients (25).

Moreover, SZ is a disease with a substantial polygenic contribution and an estimated heritability of about 80% (40). Common variants at 287 risk loci have been associated with SZ in the latest genome-wide association study (GWAS) (41). Interestingly, recent studies have identified pleiotropic genetic variants that are associated with both retinal thickness and SZ (42, 43). However, genetic investigations at the individual patient level in the field of retinal studies related to SSD are missing.

In summary, current evidence points to structural and functional retinal changes in SSD. However, the etiology of these alterations is still unknown and most previous studies have focused on either OCT or ERG (10). Thus, multimodal approaches that integrate structural and functional retinal findings as well as neuroimaging and genetics are needed to advance our understanding of retinal alterations in SSD (10). Moreover, there is a need to assess if patients with higher disease severity display more pronounced retinal alterations to explore the potential of the retina as a neuroimaging biomarker.

In the present study, we therefore performed a comprehensive multimodal analysis of the visual system in a large cross-sectional cohort of SSD patients and HC. We conducted single-layer segmentation of retinal OCT scans as well as ERG and brain MRI and applied a sparse partial least squares algorithm (SPLS) to identify a comprehensive disease signature of SSD that captures potential associations between disease severity and biological alterations of the visual system. Moreover, we aimed to investigate the association between these patterns and individual polygenic risk for SZ.

Methods

Study sample and clinical assessment

This project was part of the Clinical Deep Phenotyping study (44), an add-on study to the Munich Mental Health Biobank (ethics project number 18-716) (45) that was approved by the ethics committee of the Faculty of Medicine, LMU Munich (project numbers 20-0528 and 22-0035) and registered at the German Clinical Trials Register (DRKS, ID: DRKS00024177). It included patients with a diagnosis of SZ, schizoaffective disorder (SZA), or brief psychotic disorder as well as HC without psychiatric disorders in their lifetime according to the Mini International Neuropsychiatric Interview (46). Further study information and detailed inclusion and exclusion criteria are described in the **Supplemental Methods**. Psychotic symptom severity was assessed with the Positive and Negative Syndrome Scale (PANSS) (47), and cognitive performance, with the Brief Assessment of Cognition in Schizophrenia (BACS) (48). BACS scores were z-standardized (**Supplemental Methods**). Current antipsychotic medication was converted into chlorpromazine equivalent doses (CPZeq) (49). Participants also underwent an eye examination (**Supplemental Methods**) to measure refraction, best-corrected visual acuity (BCVA), and intraocular pressure (IOP).

Optical coherence tomography

Macular volume scans were obtained with a ZEISS CIRRUS HD-OCT 5000 device (Carl Zeiss Meditec AG, Jena, Germany) as previously described (13) (see **Supplemental Methods** for details). In short, scans were segmented by using Iowa Reference Algorithms v3.8.0 (Retinal Image Analysis Lab, Iowa Institute for Biomedical Imaging, Iowa City, IA, USA) (50-53) to obtain the thicknesses of the RNFL; GCL; IPL; inner nuclear layer (INL); outer plexiform layer (OPL); combined Henle fiber layer, ONL, and myoid zone of the photoreceptor inner segments (HFL/ONL/MZ); ellipsoid zone (EZ); photoreceptor outer segment (POS); interdigitation zone (IZ); and retinal pigment epithelium (RPE; **Figure S1A-C**); thicknesses were measured in each subfield of the Early Treatment Diabetic Retinopathy Study (ETDRS) grid (**Figure S1D**). Additionally, the MT and weighted mean layer thicknesses were calculated for the whole ETDRS grid.

Electroretinography

Photopic full-field ERG was performed with a RET*eval* electroretinograph (LKC Technologies, Inc., Gaithersburg, MD, USA). The protocol, which was obtained from Demmin et al. (28), was kindly provided by Steven Silverstein, University of Rochester Medical Center, Rochester, NY, USA, and is described in detail in the **Supplemental Methods**. Briefly, the ERG protocol included three flash ERG conditions (P_1, P_{PhNR}, P_2) that allowed us to obtain amplitudes and implicit times of a- and b-waves and the corresponding b/a ratio (**Figure S1E**). P_1 was a 100 Td·s stimulus presented at 1 Hz without background luminance; P_{PhNR} was a red stimulus presented against a blue background and was included to additionally measure the photopic negative response (PhNR) as a proxy for ganglion cell function; and P_2 had the same flash intensity as P_1 but was presented against a white background and at a frequency of 2 Hz. The protocol also included a flicker condition (P_F) to isolate the cone system (54) (**Figure S1E**).

Magnetic resonance imaging

MRI recordings were performed on a 3T Siemens MAGNETOM Prisma scanner (Siemens Healthineers AG, Erlangen, Germany) with a 32-channel head coil. T1-weighted scans were acquired by using a magnetization-prepared rapid gradient echo (MP-RAGE) sequence with an isotropic voxel size of 0.8 mm^3, 208 slices, a repetition time of 2500 ms, an echo time of 2.22 ms, a flip angle of 8°, and a field of view of 256 mm. Preprocessing and brain volume calculations were performed with NAMNIs v0.3 software (55). Jülich Atlas (56) was used to obtain whole-brain gray matter (GM) and white matter (WM) volumes and the GM and WM volumes of the following regions of interest in the left and right brain hemispheres: visual area 1 (V1; Brodman area 17), V2 (Brodman area 18), V3, V4, V5, and lateral geniculate body; volumes were calculated in mm^3 and corrected for intracranial volume. The volumes of the optic nerves were calculated by adding the respective GM and WM volumes. Furthermore, the volume of the optic chiasm was calculated with FreeSurfer (v6.0; available at: https://surfer.nmr.mgh.harvard.edu/) (57).

Genotyping and PRS calculation

Individuals were genotyped using Illumina's Global Screening Array (GSA) v3.0 at Life & Brain GmbH, Bonn, Germany. After genotype imputation (**Supplemental Methods**), genotype dosage data was used to calculate polygenic risk (PRS) for SZ (SZ-PRS) for 213 individuals corresponding to the case-control cohort used in this study based on the results of the PGC3 SZ GWAS (41). Posterior single-nucleotide polymorphism effect sizes were inferred under continuous shrinkage priors using PRS-CS (58). The global shrinkage parameter (φ) was estimated using a fully Bayesian approach (58).

Statistical analysis

To capture multivariate associations between phenotypic (i.e., clinical and sociodemographic) and biological data (OCT, ERG, MRI), we applied a sparse partial least squares (SPLS) algorithm (59) to our multimodal cohort of SSD patients and HC as implemented by Popovic et al. (60, 61). Partial least squares is an unsupervised machine learning method that uses singular value decomposition to identify pairs of weight vectors, i.e., latent variables (LVs); this approach maximizes the covariance between two different data views (60). These LVs place weights on the features of two different matrices (62), indicating how strongly and in which direction the features are associated with each other in a multivariate context (61). When given phenotypic and biological eye-related data, as in this case, partial least squares identifies signatures between these two data domains, thus generating phenotype-eye-brain signatures. SPLS additionally enforces sparsity on these weight vectors so that only the most relevant features are kept within the signatures (60, 61).

For model generation and testing, the SPLS algorithm was embedded in a 5×5-fold nested cross-validation framework (60). In brief, hyperparameters were optimized with a 40×40–point grid search on the inner CV1 layer. Significance testing of LVs was performed via permutation testing against 5000 permuted datasets on the outer CV2 layer. Feature weight stability was assessed by using 500 bootstrap samples with the optimized hyperparameters (63). Detailed information about the SPLS algorithm and machine learning

framework is provided in the **Supplemental Methods**. Individual loadings on the respective weight vectors, i.e., retina-brain and clinical phenotype scores, were compared between HC, SZA and SZ using Welch's ANOVA and the Games-Howell post hoc test. Associations between latent scores and SZ-PRS were assessed by linear regression (controlling for the first five multidimensional scaling ancestry components) within 171 cases and controls that survived quality control and were included in the SPLS analysis.

Furthermore, covariate-adjusted case-control comparisons at the level of individual OCT and ERG features were performed with generalized estimation equations (GEEs) (64), which enable the intra-individual correlation between both eyes to be accounted for (65) (**Supplemental Methods**). Age, sex, spherical equivalent, IOP, body mass index (BMI), diabetes, hypertension, and smoking status were included as covariates.

Finally, the relationship between retinal layer thicknesses and brain volumes in individuals with SSD was explored with partial Spearman correlation controlling for age and sex (**Supplemental Methods**).

Results

Cohort characteristics

The study sample comprised 103 individuals with SSD (33% females, age 39.08 ± 10.48 years, PANSS total score 49.57 ± 14.58, illness duration 13.23 ± 8.75 years, chlorpromazine equivalents 334.58 ± 282.28 mg) and 130 HC (50% females, age 33.58 ± 11.85 years; **Table 1**). The most common diagnosis among the patients was SZ (72%), followed by SZA (25%) and brief psychotic disorder (3%). The mean duration of untreated psychosis (DUP) was 24.11 months (*SD* = 37.39). Most patients (90%) were taking antipsychotic medication. 42% of patients were in symptomatic remission.

Multivariate phenotype-eye-brain signature

We applied the SPLS algorithm to capture multivariate disease-relevant patterns of the visual system. The multivariate analysis identified one significant latent variable (LV), i.e., a pair of

weight vectors (Spearman's ρ = 0.60; p < 0.001; N = 184, N_{SSD} = 80; N_{HC} = 104; **Figure 1**; **Table S1**). **Clinical phenotype pattern:** Within the vector of the clinical phenotype parameters (**Figure 1B**), the highest positive weights were found for duration of illness, age, and being affected by SSD. CPZeq, DUP, and PANSS scores also received positive weights. Among PANSS subscales, the lowest weight was found for positive symptoms. The greatest negative weight was found for being an unaffected individual, followed by the BACS composite z-score and BACS subtests. Among BACS subtests, the greatest negative weight was found for verbal memory, followed by the token motor task and symbol coding. Somatic comorbidities and cardiovascular risk factors (BMI, smoking, diabetes, and hypertension) also received smaller positive weights. The lowest weight was found for sex. **Retina-brain pattern:** The highest weights within the retina-brain vector were found for ERG features, especially b-wave implicit times. Apart from the thickness of the IZ and the POS, the thicknesses of all retinal layers were part of the retina-brain pattern: The right and left IPL thickness received the greatest (negative) weights, followed by the MT, RNFL, and HFL/ONL/MZ thickness. Fourteen out of 29 MRI features that covered the visual pathway within the brain were part of the disease signature, but these brain volume features had a much lower weighting compared to the retinal features.

To address whether the identified phenotype-eye-brain signature in SSD differed between SSD subgroups, we compared the individual loadings between HC, SZA and SZ and found significant differences between HC and SZA as well as HC and SZ for both the clinical phenotype and the retina-brain scores, but no differences between SZA and SCZ for either one (**Figure S2**; **Table S2**).

Individual disease pattern of the visual system correlates with the genetic risk.

Next, we aimed to investigate the potential connection between the SSD-relevant signature of the visual system and the underlying genetic component of the disease. This was done to investigate whether the identified SSD-relevant multivariate phenotype in the eye-brain signature is influenced not only by mediators such as enriched comorbidities but also by the

underlying disease biology. Linear regression revealed a significant association of SZ-PRS with higher individual loading on the retina-brain vector as well as higher loading on the clinical phenotype vector (both $p < 0.001$; $N = 171$; **Figure 2**; **Table S3**).

Pronounced thinning of the inner retinal layers

To provide estimates of between-group differences, we performed additional covariate-adjusted case-control comparisons. GEEs were used to compare the MT and the thicknesses of ten different retinal layers between patients and HC (**Figure 3A**; **Table S4-S6)**. The analysis revealed reduced total macular (estimate [95% CI] = −5.81 µm [−9.97, −1.66]; $q = 0.034$, where q is the false discovery rate [FDR] adjusted p value), RNFL (estimate [95% CI] = −1.49 µm [−2.64, −0.34]; $q = 0.04$), and IPL (estimate [95% CI] = −1.36 µm [−2.30, −0.43]; $q = 0.034$) thickness in SSD.

To explore whether the observed alterations followed a specific spatial pattern or differed between the right and left eye, we performed subsequent analyses for the different subfields of the ETDRS grid in those layers that were significantly altered in SSD (**Figure 3B**; **Table S7 and S8**). Thinning was slightly more pronounced in the nasal than the temporal subfields and almost symmetrical between both eyes. Only for IPL, we found discrete interactions between group and eye that indicated slightly stronger effects of SSD in the central and inner subfields of the right eye.

Altered retinal electrophysiology in SSD

In line with the structural post hoc analysis, we conducted a covariate-adjusted direct case-control comparison with the electrophysiological retinal parameters. For P_1, the a-wave amplitude was significantly less negative (estimate [95% CI] = 5.08 µV [2.64, 7.52]; $q = 0.001$) and the b-wave amplitude was significantly less positive (estimate [95% CI] = −7.40 µV [−11.43, −3.38]; $q = 0.003$) in patients with SSD than in HC (**Figure 4**; **Table S9-S11)**.

Relationship between altered retinal layers and downstream visual regions

To explore potential direct retina-brain associations and to evaluate whether the retina can in fact be considered a “window to the brain”, we calculated partial Spearman correlations

between retinal layers that were altered in SSD and downstream (sub)cortical structures of the visual pathway as well as whole brain volume within SSD patients. The highest correlations were found between RNFL thickness and volumes of the right (ρ = 0.37) and left (ρ = 0.29) optic nerves, but they were not statistically significant after FDR adjustment. All other examined retina-brain connections were weaker and not significant (**Figure S3; Table S12**).

Discussion

This study provides evidence of both microstructural and electrophysiological alterations in the visual system among individuals with SSD which are more pronounced in patients with greater disease severity. Moreover, we have established a relationship between the degree of individual disease-associated alterations of the visual system and the polygenic burden for SZ.

The applied SPLS analysis revealed a multivariate phenotype-eye-brain signature of SSD, linking phenotypic features of chronic disease and of greater disease severity (such as longer duration of illness, higher PANSS sores, higher CPZeq, and impaired cognition) to altered retinal markers (such as prolonged latencies and reduced amplitudes of ERG responses and microstructural thinning of retinal layers) and discrete changes in visual cortical areas. The multimodal retina-brain pattern was characterized by thinning of several retinal layers, with the IPL, the RNFL, and the HFL/ONL/MZ being most affected. Moreover, the signature implicated alterations of electrophysiological markers related to bipolar cell function, specifically longer b-wave implicit times, and photoreceptor function (66), aligning with the findings of previous case-control studies (27, 28, 31). Notably, there were no significant differences between SZ and SZA regarding the loadings onto the weight vectors, indicating that the revealed signature is not exclusive to a particular subgroup but rather reflects a broader phenotype of SSD (10, 67). Consistent with these results, the additional case-control OCT analysis confirmed RNFL and IPL thinning in SSD that was nearly symmetrical in both eyes, indicating a general biological effect of microstructural alterations of RGC axons in the RNFL and altered synaptic connections or branching of bipolar cells, RGCs, or amacrine cells in the IPL (68). The effects

were more nasally than temporally pronounced, which might indicate that retinal alterations in SSD are more evident within the maculopapular bundle.

The ERG investigation uncovered distinct electrophysiological alterations, i.e., lower a- and b-wave amplitudes in SSD, indicating reduced photoreceptor and bipolar cell responses to light stimuli in SSD (66). However, while lower HFL/ONL/MZ thickness had a comparatively high weight in the multivariate signature, the covariate-adjusted direct case-control comparison did not identify significant group-level differences in the thicknesses of the outer retinal layers or the INL, where the somata of photoreceptors and bipolar cells are located (68). Thus, HFL/ONL/MZ thickness could be especially affected in patients with greater disease severity. Moreover, functional changes may become apparent earlier in the course of the diseases than morphological alterations, as has been described in eye conditions such as glaucoma (69). Another (technical) hypothesis that could in part address the discrepancy between structural and functional findings is that the applied full-field ERG assesses general retinal function (54) while our OCT protocol only covered the macular center of the retina.

Previous studies have reported both reduced (26, 28) and increased (32) PhNR amplitudes in SSD, indicating potential electrophysiological alterations of RGCs (66, 70-72). In partial contrast to these findings, in the present well-powered study, while we observed RNFL thinning indicative of RGC axonal loss, no significant group effect of SSD on the PhNR, the W-ratio, or the GCL (where the RGC somata are located (68)) was found. Additionally, apart from the RNFL thickness, RGC-related parameters received only low weights in the multivariate signature.

A topic of lively discussion is whether retinal changes in SSD originate primarily in the retina itself as a result of unknown disease-driven mechanisms; are a consequence of retrograde transsynaptic degeneration (3, 73); or are mediated by other variables that are enriched in individuals with SSD, such as cardiovascular risk factors (3, 13, 74-78). In the present study, we identified several microstructural and electrophysiological alterations of the retina in SSD that were highly robust even though we controlled for a series of covariates associated with retinal thickness, such as age, sex, spherical equivalent, IOP, BMI, diabetes,

hypertension, and smoking (3, 79, 80). Still, there remains a possibility that other (environmental) factors could in part mediate the observed retinal thinning. For example, social deprivation was shown to be associated with thinner inner retinal layers in the general population (81).

Post hoc analyses revealed no statistically significant correlations between altered retinal structures and downstream visual regions or total GM or WM volume in patients (**Figure S3**), indicating that structural retinal alterations in SSD are not directly reflected by structural changes of the brain. These findings challenge the hypothesis that the observed retinal thinning is mainly due to retrograde processes in the classic visual pathway, such as transsynaptic degeneration. Instead, retinal and cerebral changes in SSD might occur independently but be due to common, as yet unknown mechanisms (1).

Given the recent evidence of genetic pleiotropy between retinal thickness and SZ (42, 43), the observation of IPL thinning also in unaffected first-degree relatives of SZ patients (82) as well as that electroretinographic alterations have also been described in offspring of individuals diagnosed with SZ and other psychiatric diseases (83-86), an important question was how the observed alterations of the visual system in SSD relate to the polygenic architecture of the diseases. Fascinatingly, our genetic analysis uncovered an association between individual loadings on the retina-dominated visual system signature and the individual polygenetic risk for SZ. Although these findings do not allow causal conclusions, they indicate that retinal alterations in SSD are, to some extent, influenced by yet unidentified genetically driven mechanisms of the complex polygenic disease. Notably, SZ-PRS explained only a small part of the variance in retina-brain scores (**Figure 2**). Consistent with the multifactorial etiology of SSD (67, 87, 88), non-genetic risk factors are likely also implicated in the pathophysiological processes driving alterations in retinal structure and function in SSD.

This study has several limitations. First, an additional effect of antipsychotics on the retina cannot be excluded. For example, flash ERG responses in healthy volunteers were altered after intake of antipsychotic medications (89-94). However, the significant link between SZ-PRS and the individual loadings on the revealed visual system signature strongly argues

against an effect solely of medical treatment and supports the hypothesis that, at least in part, primary disease mechanisms affect retinal structure and function in SSD. Second, because of its cross-sectional nature, the study does not provide direct evidence on the longitudinal development and stability of retinal alterations in SSD. Third, the specificity of the observed retinal alterations for SSD should be addressed in future studies that include individuals with other psychiatric diagnoses. Fourth, there might be non-monotonic relationships between some clinical features and retinal alterations (18) that were not captured by the SPLS algorithm. Fifth, the comparability of our results with previous OCT studies might be limited by our use of a different segmentation algorithm that combined the ONL and the myoid zone of the inner segments into a single layer. Sixth, although the applied handheld ERG is far more feasible in clinical research settings and non-invasive skin electrodes are better accepted by study participants, conventional devices using corneal electrodes have a better signal-to-noise ratio (95) and may therefore be more sensitive to subtle changes.

In summary, our study provides evidence that microstructural and functional alterations of the retina in SSD are associated with disease duration and severity as well as with the individual genetic disease risk. Our findings therefore indicate that retinal alterations in SSD have both state and trait (10) aspects. Moreover, the revealed association with genetic risk for SZ highlights the potential of retinal alterations as an endophenotype candidate in SSD (67). In this regard, as an accessible part of the central nervous system (CNS), the retina may contribute to a better understanding of the neurobiological mechanisms of SSD. Apart from scientific applications, it remains to be investigated to what extent retinal neuroimaging and electrophysiology could complement established investigations in clinical settings, for example for subgroup identification or as a cost-effective screening tool for CNS alterations over time.

Data availability

Upon publication of this article, the de-identified data of this study will be made available in the Zenodo repository at https://doi.org/10.5281/zenodo.7510469 *(link accessible after acceptance of the manuscript)*.

CDP Working Group

Valéria de Almeida, Stephanie Behrens, Emanuel Boudriot, Mattia Campana, Fanny Dengl, Peter Falkai, Laura E. Fischer, Nadja Gabellini, Vanessa Gabriel, Thomas Geyer, Katharina Hanken, Alkomiet Hasan, Genc Hasanaj, Georgios Ioannou, Iris Jäger, Sylvia de Jonge, Temmuz Karali, Susanne Karch, Berkhan Karslı, Daniel Keeser, Christoph Kern, Nicole Klimas, Lenka Krčmář, Julian Melcher, Matin Mortazavi, Joanna Moussiopoulou, Karin Neumeier, Frank Padberg, Boris Papazov, Sergi Papiol, Pauline Pingen, Oliver Pogarell, Siegfried Priglinger, Florian J. Raabe, Lukas Roell, Moritz J. Rossner, Andrea Schmitt, Susanne Schmölz, Enrico Schulz, Benedikt Schworm, Elias Wagner, Sven Wichert, Vladislav Yakimov, Peter Zill (collaborators listed alphabetically). Main contact: Florian J. Raabe, Department of Psychiatry and Psychotherapy, LMU University Hospital, LMU Munich, 80336 Munich, Germany.

Acknowledgments

EB, VG, and PP were supported by doctoral scholarships from the Faculty of Medicine, LMU Munich, Munich, Germany. DP and FJR were supported by the Else Kröner-Fresenius Foundation (Research College “Translational Psychiatry”) for their Residency/PhD track at the International Max Planck Research School for Translational Psychiatry (IMPRS-TP), Munich, Germany. FJR and ECS were supported by the Munich Clinician Scientist Program (MCSP) of the Faculty of Medicine, LMU Munich, Munich, Germany (FöFoLe 009/2019 and Advanced Track 01/2021, respectively). FJR received funding from the Lisa Oehler-Stiftung (2022–2024). EW was supported by the Förderprogramm für Forschung und Lehre (FöFoLe), University Hospital, LMU Munich (registration number 1083). PF and AH were supported by the Federal Ministry of Education and Research (Bundesministerium für Bildung und Forschung [BMBF]) within the initial phase of the German Center for Mental Health (DZPG; grant FKZ 01EE2303A and 01EE2303F to PF and FKZ 01EE2303C to AH). PF, GH, and VY received funding from the BMBF within the Era-Net Neuron project GDNF_UpReg (FKZ 01EW2206).

DK, FJR, and EW led the general design and conceptualization of the *Munich Clinical Deep Phenotyping (CDP) study* with supervision by AH, PF, AS, and OP. This study was conceptualized by EB, VG, DP, and FJR. JM, EW, and VY trained staff in diagnostic and clinical assessments. Eye examinations were performed by EB, VG, and PP under the ophthalmologic supervision of CK, SiP, and BS. MRI acquisition and processing was performed by GH and LR. Genotyping and genetic analysis was conducted by SeP, FJR, ECS, and VY. SPLS analysis was performed by DP. All other statistical analyses were performed by EB. Data visualization was performed by EB, VG, DP, FJR, and SX. EB, VG, and FJR wrote the first draft of the manuscript. All authors contributed to and approved the final version of the manuscript. Supervision of the work by FJR.

The authors thank all participants for their support. Furthermore, they thank all researchers and clinical and administrative staff from the Departments of Ophthalmology and Psychiatry and Psychotherapy at the University Hospital, LMU Munich, Munich, Germany, for their help to conduct this study; Steven Silverstein, University of Rochester Medical Center, Rochester, NY, USA, who the kindly provided the ERG protocol; and Jacquie Klesing, BMedSci (Hons), Board-certified Editor in the Life Sciences (ELS), for editing assistance with the manuscript.

Conflict of Interest

AH received speaker fees from AbbVie, Advanz, Janssen, Otsuka, Lundbeck, Rovi, and Recordati and was a member of the advisory boards of these companies and Boehringer-Ingelheim. AS was an honorary speaker for TAD Pharma and Roche and a member of the advisory boards for Roche. BS received speaker fees from Novartis Pharma GmbH. CK received speaker fees from Bayer AG and received grants from Zeiss Meditech outside the submitted work. EW has been invited to advisory boards by Recordati. OP received speaker fees from Lundbeck, Otsuka, Takeda, and Janssen and was a member of the advisory boards of Lundbeck and Janssen. PF received speaker fees from Boehringer-Ingelheim, Janssen, Otsuka, Lundbeck, Recordati, and Richter and was a member of the advisory boards of these

companies and Rovi. SiP received speaker fees and/or travel expenses from Novartis Pharma GmbH, Oertli AG, Bayer AG, Alcon Pharma GmbH, and Pharm-Allergan GmbH. Reported disclosures from above authors are unrelated to this study. All other authors report no biomedical financial interests or potential conflicts of interest.

Supplementary Material

- Supplement (separate PDF file)
    - Supplemental Figures S1, S2, and S3
    - Supplemental Methods
- Key Resources Table (separate Excel File)
- Supplemental Tables (separate Excel File)
    - Tables S1-S12

References

1. Gonzalez-Diaz JM, Radua J, Sanchez-Dalmau B, Camos-Carreras A, Zamora DC, Bernardo M (2022): Mapping Retinal Abnormalities in Psychosis: Meta-analytical Evidence for Focal Peripapillary and Macular Reductions. *Schizophr Bull*.
2. Komatsu H, Onoguchi G, Jerotic S, Kanahara N, Kakuto Y, Ono T, et al. (2022): Retinal layers and associated clinical factors in schizophrenia spectrum disorders: a systematic review and meta-analysis. *Mol Psychiatry*.
3. Silverstein SM, Fradkin SI, Demmin DL (2020): Schizophrenia and the retina: Towards a 2020 perspective. *Schizophr Res*. 219:84-94.
4. Heavner W, Pevny L (2012): Eye development and retinogenesis. *Cold Spring Harb Perspect Biol*. 4.
5. Sadler TW (2018): Eye. *Langman's Medical Embryology*, 14th ed. Philadelphia, PA, USA: Wolters Kluwer, pp 360-369.
6. London A, Benhar I, Schwartz M (2013): The retina as a window to the brain-from eye research to CNS disorders. *Nat Rev Neurol*. 9:44-53.
7. Marchesi N, Fahmideh F, Boschi F, Pascale A, Barbieri A (2021): Ocular Neurodegenerative Diseases: Interconnection between Retina and Cortical Areas. *Cells*. 10.
8. Schönfeldt-Lecuona C, Kregel T, Schmidt A, Pinkhardt EH, Lauda F, Kassubek J, et al. (2016): From Imaging the Brain to Imaging the Retina: Optical Coherence Tomography (OCT) in Schizophrenia. *Schizophr Bull*. 42:9-14.
9. Aumann S, Donner S, Fischer J, Müller F (2019): Optical Coherence Tomography (OCT): Principle and Technical Realization. In: Bille JF, editor. *High Resolution Imaging in Microscopy and Ophthalmology: New Frontiers in Biomedical Optics*. Cham, Switzerland: Springer International Publishing, pp 59-85.
10. Komatsu H, Onoguchi G, Silverstein SM, Jerotic S, Sakuma A, Kanahara N, et al. (2023): Retina as a potential biomarker in schizophrenia spectrum disorders: a systematic review and meta-analysis of optical coherence tomography and electroretinography. *Molecular Psychiatry*.

11. Wagner SK, Cortina-Borja M, Silverstein SM, Zhou Y, Romero-Bascones D, Struyven RR, et al. (2023): Association Between Retinal Features From Multimodal Imaging and Schizophrenia. *JAMA Psychiatry*. 80:478-487.
12. Domagała A, Domagała L, Kopiś-Posiej N, Harciarek M, Krukow P (2023): Differentiation of the retinal morphology aging trajectories in schizophrenia and their associations with cognitive dysfunctions. *Frontiers in Psychiatry*. 14.
13. Boudriot E, Schworm B, Slapakova L, Hanken K, Jäger I, Stephan M, et al. (2023): Optical coherence tomography reveals retinal thinning in schizophrenia spectrum disorders. *European Archives of Psychiatry and Clinical Neuroscience*. 273:575-588.
14. Lee WW, Tajunisah I, Sharmilla K, Peyman M, Subrayan V (2013): Retinal nerve fiber layer structure abnormalities in schizophrenia and its relationship to disease state: evidence from optical coherence tomography. *Invest Ophthalmol Vis Sci*. 54:7785-7792.
15. Blose BA, Lai A, Crosta C, Thompson JL, Silverstein SM (2023): Retinal Neurodegeneration as a Potential Biomarker of Accelerated Aging in Schizophrenia Spectrum Disorders. *Schizophr Bull*. 49:1316-1324.
16. Lai A, Crosta C, Loftin M, Silverstein SM (2020): Retinal structural alterations in chronic versus first episode schizophrenia spectrum disorders. *Biomarkers in Neuropsychiatry*. 2:100013.
17. Ascaso FJ, Rodriguez-Jimenez R, Cabezón L, López-Antón R, Santabárbara J, De la Cámara C, et al. (2015): Retinal nerve fiber layer and macular thickness in patients with schizophrenia: Influence of recent illness episodes. *Psychiatry Research*. 229:230-236.
18. Alizadeh M, Delborde Y, Ahmadpanah M, Seifrabiee MA, Jahangard L, Bazzazi N, et al. (2021): Non-linear associations between retinal nerve fibre layer (RNFL) and positive and negative symptoms among men with acute and chronic schizophrenia spectrum disorder. *Journal of Psychiatric Research*. 141:81-91.
19. Wolfers T, Doan NT, Kaufmann T, Alnæs D, Moberget T, Agartz I, et al. (2018): Mapping the Heterogeneous Phenotype of Schizophrenia and Bipolar Disorder Using Normative Models. *JAMA Psychiatry*. 75:1146-1155.
20. Kango A, Grover S, Gupta V, Sahoo S, Nehra R (2023): A comparative study of retinal layer changes among patients with schizophrenia and healthy controls. *Acta Neuropsychiatr*. 35:165-176.
21. Petzold A, Balcer LJ, Calabresi PA, Costello F, Frohman TC, Frohman EM, et al. (2017): Retinal layer segmentation in multiple sclerosis: a systematic review and meta-analysis. *Lancet Neurol*. 16:797-812.
22. Oberwahrenbrock T, Traber GL, Lukas S, Gabilondo I, Nolan R, Songster C, et al. (2018): Multicenter reliability of semiautomatic retinal layer segmentation using OCT. *Neurol Neuroimmunol Neuroinflamm*. 5:e449.
23. Samani NN, Proudlock FA, Siram V, Suraweera C, Hutchinson C, Nelson CP, et al. (2018): Retinal Layer Abnormalities as Biomarkers of Schizophrenia. *Schizophr Bull*. 44:876-885.
24. Schönfeldt-Lecuona C, Kregel T, Schmidt A, Kassubek J, Dreyhaupt J, Freudenmann RW, et al. (2020): Retinal single-layer analysis with optical coherence tomography (OCT) in schizophrenia spectrum disorder. *Schizophr Res*. 219:5-12.
25. Bannai D, Lizano P, Kasetty M, Lutz O, Zeng V, Sarvode S, et al. (2020): Retinal layer abnormalities and their association with clinical and brain measures in psychotic disorders: A preliminary study. *Psychiatry Res Neuroimaging*. 299:111061.

26. Friedel EBN, Hahn HT, Maier S, Kuchlin S, Reich M, Runge K, et al. (2022): Structural and functional retinal alterations in patients with paranoid schizophrenia. *Transl Psychiatry*. 12:402.
27. Hébert M, Mérette C, Gagné AM, Paccalet T, Moreau I, Lavoie J, et al. (2020): The Electroretinogram May Differentiate Schizophrenia From Bipolar Disorder. *Biol Psychiatry*. 87:263-270.
28. Demmin DL, Davis Q, Roché M, Silverstein SM (2018): Electroretinographic anomalies in schizophrenia. *J Abnorm Psychol*. 127:417-428.
29. Balogh Z, Benedek G, Kéri S (2008): Retinal dysfunctions in schizophrenia. *Prog Neuropsychopharmacol Biol Psychiatry*. 32:297-300.
30. Warner R, Laugharne J, Peet M, Brown L, Rogers N (1999): Retinal function as a marker for cell membrane omega-3 fatty acid depletion in schizophrenia: a pilot study. *Biol Psychiatry*. 45:1138-1142.
31. Hébert M, Mérette C, Paccalet T, Émond C, Gagné AM, Sasseville A, et al. (2015): Light evoked potentials measured by electroretinogram may tap into the neurodevelopmental roots of schizophrenia. *Schizophr Res*. 162:294-295.
32. Moghimi P, Torres Jimenez N, McLoon LK, Netoff TI, Lee MS, MacDonald A, 3rd, et al. (2020): Electoretinographic evidence of retinal ganglion cell-dependent function in schizophrenia. *Schizophr Res*. 219:34-46.
33. Bernardin F, Schwitzer T, Schwan R, Angioi-Duprez K, Ligier F, Bourion-Bedes S, et al. (2022): Altered central vision and amacrine cells dysfunction as marker of hypodopaminergic activity in treated patients with schizophrenia. *Schizophr Res*. 239:134-141.
34. Bernardin F, Schwitzer T, Angioi-Duprez K, Giersch A, Jansen C, Schwan R, et al. (2020): Retinal ganglion cells dysfunctions in schizophrenia patients with or without visual hallucinations. *Schizophr Res*. 219:47-55.
35. Türközer HB, Lizano P, Adhan I, Ivleva EI, Lutz O, Zeng V, et al. (2022): Regional and Sex-Specific Alterations in the Visual Cortex of Individuals With Psychosis Spectrum Disorders. *Biol Psychiatry*. 92:396-406.
36. Zhuo C, Ji F, Xiao B, Lin X, Chen C, Jiang D, et al. (2020): Antipsychotic agent-induced deterioration of the visual system in first-episode untreated patients with schizophrenia maybe self-limited: Findings from a secondary small sample follow-up study based on a pilot follow-up study. *Psychiatry Res*. 286:112906.
37. Zhuo C, Xiao B, Chen C, Jiang D, Li G, Ma X, et al. (2020): Antipsychotic agents deteriorate brain and retinal function in schizophrenia patients with combined auditory and visual hallucinations: A pilot study and secondary follow-up study. *Brain Behav*. 10:e01611.
38. Zhuo C, Xiao B, Chen C, Jiang D, Li G, Ma X, et al. (2021): Abberant inverted U-shaped brain pattern and trait-related retinal impairment in schizophrenia patients with combined auditory and visual hallucinations: a pilot study. *Brain Imaging Behav*. 15:738-747.
39. Zhuo C, Xiao B, Ji F, Lin X, Jiang D, Tian H, et al. (2021): Patients with first-episode untreated schizophrenia who experience concomitant visual disturbances and auditory hallucinations exhibit co-impairment of the brain and retinas-a pilot study. *Brain Imaging Behav*. 15:1533-1541.
40. Hilker R, Helenius D, Fagerlund B, Skytthe A, Christensen K, Werge TM, et al. (2018): Heritability of Schizophrenia and Schizophrenia Spectrum Based on the Nationwide Danish Twin Register. *Biol Psychiatry*. 83:492-498.

41. Trubetskoy V, Pardinas AF, Qi T, Panagiotaropoulou G, Awasthi S, Bigdeli TB, et al. (2022): Mapping genomic loci implicates genes and synaptic biology in schizophrenia. *Nature*. 604:502-508.
42. Gao XR, Huang H, Kim H (2018): Genome-wide association analyses identify 139 loci associated with macular thickness in the UK Biobank cohort. *Human Molecular Genetics*. 28:1162-1172.
43. Zhao B, Li Y, Fan Z, Wu Z, Shu J, Yang X, et al. (2023): Eye-brain connections revealed by multimodal retinal and brain imaging genetics in the UK Biobank. *medRxiv*.
44. Krčmář L, Jäger I, Boudriot E, Hanken K, Gabriel V, Melcher J, et al. (2023): The multimodal Munich Clinical Deep Phenotyping study to bridge the translational gap in severe mental illness treatment research. *Frontiers in Psychiatry*. 14.
45. Kalman JL, Burkhardt G, Adorjan K, Barton BB, De Jonge S, Eser-Valeri D, et al. (2022): Biobanking in everyday clinical practice in psychiatry—The Munich Mental Health Biobank. *Frontiers in Psychiatry*. 13.
46. Sheehan DV, Lecrubier Y, Sheehan KH, Amorim P, Janavs J, Weiller E, et al. (1998): The Mini-International Neuropsychiatric Interview (M.I.N.I.): the development and validation of a structured diagnostic psychiatric interview for DSM-IV and ICD-10. *J Clin Psychiatry*. 59 Suppl 20:22-33;quiz 34-57.
47. Kay SR, Fiszbein A, Opler LA (1987): The Positive and Negative Syndrome Scale (PANSS) for Schizophrenia. *Schizophrenia Bulletin*. 13:261-276.
48. Keefe RSE, Goldberg TE, Harvey PD, Gold JM, Poe MP, Coughenour L (2004): The Brief Assessment of Cognition in Schizophrenia: reliability, sensitivity, and comparison with a standard neurocognitive battery. *Schizophrenia Research*. 68:283-297.
49. Leucht S, Samara M, Heres S, Davis JM (2016): Dose Equivalents for Antipsychotic Drugs: The DDD Method. *Schizophr Bull*. 42 Suppl 1:S90-94.
50. Kang L, Xiaodong W, Chen DZ, Sonka M (2006): Optimal Surface Segmentation in Volumetric Images-A Graph-Theoretic Approach. *IEEE Transactions on Pattern Analysis and Machine Intelligence*. 28:119-134.
51. Garvin MK, Abramoff MD, Wu X, Russell SR, Burns TL, Sonka M (2009): Automated 3-D intraretinal layer segmentation of macular spectral-domain optical coherence tomography images. *IEEE Trans Med Imaging*. 28:1436-1447.
52. Abramoff MD, Garvin MK, Sonka M (2010): Retinal imaging and image analysis. *IEEE Rev Biomed Eng*. 3:169-208.
53. Terry L, Cassels N, Lu K, Acton JH, Margrain TH, North RV, et al. (2016): Automated Retinal Layer Segmentation Using Spectral Domain Optical Coherence Tomography: Evaluation of Inter-Session Repeatability and Agreement between Devices. *PLOS ONE*. 11:e0162001.
54. Robson AG, Frishman LJ, Grigg J, Hamilton R, Jeffrey BG, Kondo M, et al. (2022): ISCEV Standard for full-field clinical electroretinography (2022 update). *Doc Ophthalmol*. 144:165-177.
55. Karali T, Padberg F, Kirsch V, Stoecklein S, Falkai P, Keeser D (2021): NAMNIs: Neuromodulation And Multimodal NeuroImaging software (0.3). *Zenodo*.
56. Eickhoff SB, Paus T, Caspers S, Grosbras MH, Evans AC, Zilles K, et al. (2007): Assignment of functional activations to probabilistic cytoarchitectonic areas revisited. *Neuroimage*. 36:511-521.

57. Fischl B, Salat DH, Busa E, Albert M, Dieterich M, Haselgrove C, et al. (2002): Whole brain segmentation: automated labeling of neuroanatomical structures in the human brain. *Neuron*. 33:341-355.
58. Ge T, Chen CY, Ni Y, Feng YA, Smoller JW (2019): Polygenic prediction via Bayesian regression and continuous shrinkage priors. *Nat Commun*. 10:1776.
59. Wold H (1982): Soft modelling: the basic design and some extensions. In: Jöreskog KG, Wold HOA, editors. *Systems under indirect observation: Part II*. Amsterdam, pp 1–54.
60. Popovic D, Ruef A, Dwyer DB, Antonucci LA, Eder J, Sanfelici R, et al. (2020): Traces of Trauma: A Multivariate Pattern Analysis of Childhood Trauma, Brain Structure, and Clinical Phenotypes. *Biol Psychiatry*. 88:829-842.
61. Monteiro JM, Rao A, Shawe-Taylor J, Mourão-Miranda J, Alzheimer's Disease Initiative (2016): A multiple hold-out framework for Sparse Partial Least Squares. *J Neurosci Methods*. 271:182-194.
62. McIntosh AR, Lobaugh NJ (2004): Partial least squares analysis of neuroimaging data: applications and advances. *NeuroImage*. 23 Suppl 1:S250-263.
63. Krishnan A, Williams LJ, McIntosh AR, Abdi H (2011): Partial Least Squares (PLS) methods for neuroimaging: a tutorial and review. *NeuroImage*. 56:455-475.
64. Liang K-Y, Zeger SL (1986): Longitudinal data analysis using generalized linear models. *Biometrika*. 73:13-22.
65. Ying GS, Maguire MG, Glynn R, Rosner B (2017): Tutorial on Biostatistics: Linear Regression Analysis of Continuous Correlated Eye Data. *Ophthalmic Epidemiol*. 24:130-140.
66. Pasmanter N, Petersen-Jones SM (2020): A review of electroretinography waveforms and models and their application in the dog. *Vet Ophthalmol*. 23:418-435.
67. Gottesman, II, Gould TD (2003): The endophenotype concept in psychiatry: etymology and strategic intentions. *Am J Psychiatry*. 160:636-645.
68. Gregg RG, Singer J, Kamermans M, McCall MA, Massey SC (2022): Function and Anatomy of the Mammalian Retina. In: Sadda S, Schachat A, Wilkinson C, Hinton D, Wiedemann P, Freund KB, et al., editors. *Ryan's Retina*, 7th ed: Elsevier, pp 378-420.
69. Banitt MR, Ventura LM, Feuer WJ, Savatovsky E, Luna G, Shif O, et al. (2013): Progressive loss of retinal ganglion cell function precedes structural loss by several years in glaucoma suspects. *Invest Ophthalmol Vis Sci*. 54:2346-2352.
70. Machida S (2012): Clinical Applications of the Photopic Negative Response to Optic Nerve and Retinal Diseases. *Journal of Ophthalmology*. 2012:397178.
71. Marmoy OR, Viswanathan S (2021): Clinical electrophysiology of the optic nerve and retinal ganglion cells. *Eye*. 35:2386-2405.
72. Prencipe M, Perossini T, Brancoli G, Perossini M (2020): The photopic negative response (PhNR): measurement approaches and utility in glaucoma. *International Ophthalmology*. 40:3565-3576.
73. Adámek P, Langová V, Horáček J (2022): Early-stage visual perception impairment in schizophrenia, bottom-up and back again. *Schizophrenia*. 8:27.
74. Bernardo M, Cañas F, Banegas JR, Casademont J, Riesgo Y, Varela C (2009): Prevalence and awareness of cardiovascular risk factors in patients with schizophrenia: A cross-sectional study in a low cardiovascular disease risk geographical area. *European Psychiatry*. 24:431-441.
75. Correll CU, Robinson DG, Schooler NR, Brunette MF, Mueser KT, Rosenheck RA, et al. (2014): Cardiometabolic Risk in Patients With First-Episode Schizophrenia Spectrum Disorders: Baseline Results From the RAISE-ETP Study. *JAMA Psychiatry*. 71:1350-1363.

626 76. de Leon J, Diaz FJ (2005): A meta-analysis of worldwide studies demonstrates an
627 association between schizophrenia and tobacco smoking behaviors. *Schizophrenia Research*.
628 76:135-157.
629 77. McDaid TM, Smyth S (2015): Metabolic abnormalities among people diagnosed with
630 schizophrenia: a literature review and implications for mental health nurses. *Journal of*
631 *Psychiatric and Mental Health Nursing*. 22:157-170.
632 78. Correll CU, Solmi M, Veronese N, Bortolato B, Rosson S, Santonastaso P, et al. (2017):
633 Prevalence, incidence and mortality from cardiovascular disease in patients with pooled and
634 specific severe mental illness: a large-scale meta-analysis of 3,211,768 patients and
635 113,383,368 controls. *World Psychiatry*. 16:163-180.
636 79. De Clerck EEB, Schouten JSAG, Berendschot TTJM, Goezinne F, Dagnelie PC, Schaper
637 NC, et al. (2018): Macular thinning in prediabetes or type 2 diabetes without diabetic
638 retinopathy: the Maastricht Study. *Acta Ophthalmologica*. 96:174-182.
639 80. Patel PJ, Foster PJ, Grossi CM, Keane PA, Ko F, Lotery A, et al. (2016): Spectral-Domain
640 Optical Coherence Tomography Imaging in 67 321 Adults: Associations with Macular
641 Thickness in the UK Biobank Study. *Ophthalmology*. 123:829-840.
642 81. Khawaja AP, Chua S, Hysi PG, Georgoulas S, Currant H, Fitzgerald TW, et al. (2020):
643 Comparison of Associations with Different Macular Inner Retinal Thickness Parameters in a
644 Large Cohort: The UK Biobank. *Ophthalmology*. 127:62-71.
645 82. Kurtulmus A, Elbay A, Parlakkaya FB, Kilicarslan T, Ozdemir MH, Kirpinar I (2020): An
646 investigation of retinal layer thicknesses in unaffected first-degree relatives of schizophrenia
647 patients. *Schizophr Res*. 218:255-261.
648 83. Peredo R, Gagné AM, Gilbert E, Hébert M, Maziade M, Mérette C (2020):
649 Electroretinography may reveal cognitive impairment among a cohort of subjects at risk of a
650 major psychiatric disorder. *Psychiatry Res*. 291:113227.
651 84. Moreau I, Hébert M, Maziade M, Painchaud A, Mérette C (2022): The
652 Electroretinogram as a Potential Biomarker of Psychosis in Children at Familial Risk.
653 *Schizophrenia Bulletin Open*. 3.
654 85. Gagné AM, Moreau I, St-Amour I, Marquet P, Maziade M (2020): Retinal function
655 anomalies in young offspring at genetic risk of schizophrenia and mood disorder: The meaning
656 for the illness pathophysiology. *Schizophr Res*. 219:19-24.
657 86. Maziade M, Bureau A, Jomphe V, Gagné AM (2022): Retinal function and preclinical
658 risk traits in children and adolescents at genetic risk of schizophrenia and bipolar disorder.
659 *Prog Neuropsychopharmacol Biol Psychiatry*. 112:110432.
660 87. Wahbeh MH, Avramopoulos D (2021): Gene-Environment Interactions in
661 Schizophrenia: A Literature Review. *Genes (Basel)*. 12.
662 88. Hanson DR, Gottesman II (2005): Theories of schizophrenia: a genetic-inflammatory-
663 vascular synthesis. *BMC Medical Genetics*. 6:7.
664 89. Holopigian K, Clewner L, Seiple W, Kupersmith MJ (1994): The effects of dopamine
665 blockade on the human flash electroretinogram. *Documenta Ophthalmologica*. 86:1-10.
666 90. Bartel P, Blom M, Robinson E, Van Der Meyden C, De Sommers K, Becker P (1990): The
667 effects of levodopa and haloperidol on flash and pattern ERGs and VEPs in normal humans.
668 *Documenta Ophthalmologica*. 76:55-64.
669 91. Bartel P, Blom M, Robinson E, Van der Meyden C, Sommers DO, Becker P (1990):
670 Effects of chlorpromazine on pattern and flash ERGs and VEPs compared to oxazepam and to
671 placebo in normal subjects. *Electroencephalogr Clin Neurophysiol*. 77:330-339.

672 92. Filip V, Balík J (1978): Possible indication of dopaminergic blockade in man by
673 electroretinography. *Int Pharmacopsychiatry*. 13:151-156.
674 93. Perossini M, Fornaro P (1990): Electroretinographic effects induced in humans by
675 psychopharmacologic agents. *Documenta Ophthalmologica*. 75:1-6.
676 94. Fornaro P, et al. (1984): Electroretinography (ERG) as a tool of investigation on
677 dopaminergic activity in man. *Research Communications in Psychology, Psychiatry &*
678 *Behavior*. 9:307-323.
679 95. You JY, Dorfman AL, Gauvin M, Vatcher D, Polomeno RC, Little JM, et al. (2023):
680 Comparing the RETeval® portable ERG device with more traditional tabletop ERG systems in
681 normal subjects and selected retinopathies. *Documenta Ophthalmologica*. 146:137-150.
682

Figures

Figure 1. Multidimensional phenotype-eye-brain signature as identified by the sparse partial least squares algorithm

Illustration of **(A)** the biological (eye-related) vector and **(B)** the phenotypic vector of the identified latent variable (LV; Spearman's $\rho = 0.60$; $p < 0.001$; $N = 184$, $N_{SSD} = 80$; $N_{HC} = 104$). The bars visualize the direction and values of the weights assigned to the relevant features incorporated into the LV by the sparse partial least squares algorithm. Data of the right (OD, R) and left (OS, L) eye are presented separately; the latter are shown in a hatched pattern. Features where the weight of only one eye was included in the LV are written in a thinner, light gray font.

Abbreviations: BMI, body mass index; CPZeq, chlorpromazine equivalent dose; DUP, duration of untreated psychosis; EZ, ellipsoid zone; GCL, ganglion cell layer; GM, gray matter; HC, healthy control; HFL/ONL/MZ, Henle-fiber layer, outer nuclear layer, and myoid zone; INL, inner nuclear layer; IOP, intraocular pressure; IPL, inner plexiform layer; OD, oculus dexter (right eye); OS, oculus sinister (left eye); PhNR, photopic negative response; RNFL, retinal nerve fiber layer; RPE, retinal pigment epithelium; SEQ, spherical equivalent; SSD, schizophrenia spectrum disorder; WM, white matter

Figure 2. Significant association between polygenic risk for schizophrenia and individual loadings on the phenotype-eye-brain signature

(A) Association between schizophrenia polygenic risk scores (SZ-PRS) and retina-brain scores (R^2_{adj} = 0.058; p < 0.001). **(B)** Association between SZ-PRS and clinical phenotype scores (R^2_{adj} = 0.109; p < 0.001). N = 171. Red lines represent the predicted values as obtained from linear regression models; gray area indicates the 95% confidence interval; points represent the raw data.

Figure 3. Thinner retinal layers in schizophrenia spectrum disorders as shown by optical coherence tomography

(A) Comparison of mean thicknesses of retinal layers in the whole 6-mm–diameter area of the Early Treatment Diabetic Retinopathy Study (ETDRS) grid between the healthy control group (gray) and individuals with schizophrenia spectrum disorders (SSD; red), illustrated by combined box, density, and scatterplots. Shown are the total macular thickness (q = 0.034, where q is the false discovery rate-adjusted p value) and the following layers: retinal nerve fiber layer (RNFL; q = 0.04), ganglion cell layer (q = 0.439), inner plexiform layer (IPL; q = 0.034), inner nuclear layer (q = 0.614), outer plexiform layer (q = 0.614), combined Henle fiber layer/outer nuclear layer/myoid zone (q = 0.142), ellipsoid zone (q = 0.439), photoreceptor outer segment (POS; q = 0.614), interdigitation zone (q = 0.614) and retinal pigment epithelium (q = 0.614). Data points represent individual eyes. Groups were compared with generalized estimation equations to control for age, sex, spherical equivalent (SphE), intraocular pressure (IOP), body mass index (BMI), diabetes, hypertension, and smoking status. N_{SSD} = 96, n_{SSD} = 182, N_{HC} = 128, n_{HC} = 250. *q < 0.05. **(B)** Maps of the right (OD) and left eye (OS) depicting the marginal effect of SSD in µm on each subfield of the ETDRS grid in overall macular thickness, RNFL, and IPL, as obtained with generalized estimation equations to control for age, sex, SphE, IOP, BMI, diabetes, hypertension, smoking status, eye, and including an interaction between eye and group. Statistically significant effects are highlighted in red. N_{SSD} = 96, n_{SSD} = 182, N_{HC} = 128, n_{HC} = 250. *p < 0.05.

Abbreviations: EZ, ellipsoid zone; GCL, ganglion cell layer; HFL/ONL/MZ, Henle fiber layer/outer nuclear layer/myoid zone of photoreceptor inner segments; IN, inner nasal subfield; IPL, inner plexiform layer; IZ, interdigitation zone; *N*, number of participants; *n*, number of eyes; OD, oculus dexter (right eye); OPL, outer plexiform layer; OS, oculus sinister (left eye); POS, photoreceptor outer segment; *q,* false discovery rate-adjusted *p* value; RNFL, retinal nerve fiber layer; RPE, retinal pigment epithelium

Figure 4. Altered photoreceptor and bipolar cell responses in schizophrenia spectrum disorders

Comparison of electroretinography (ERG) measures between patients with schizophrenia spectrum disorders and healthy controls (HC) for four photopic conditions (P_1: N_{SSD} = 96, n_{SSD} = 182, N_{HC} = 124, n_{HC} = 241; P_{PhNR}: N_{SSD} = 92, n_{SSD} = 176, N_{HC} = 118, n_{HC} = 219; P_2: N_{SSD} = 98, n_{SSD} = 178, N_{HC} = 123, n_{HC} = 228; and P_F: N_{SSD} = 97, n_{SSD} = 185, N_{HC} = 125, n_{HC} = 246), illustrated with combined box, density, and scatterplots. Shown are **(A)** a-wave and **(B)** b-wave amplitudes, **(C)** a-wave and **(D)** b-wave implicit times, and **(E)** the b/a ratio for P_1, P_{PhNR}, and P_2; **(F)** the photopic negative response amplitudes (left) and the W-ratio (right) for P_{PhNR}; and **(G)** both the underlying fundamental and the reconstructed waveform implicit times (left) and amplitudes (right) in the flicker ERG test (P_F). Data points represent individual eyes. *q < 0.05. p values were obtained with generalized estimation equations to control for age, sex, spherical equivalent, intraocular pressure, body mass index, diabetes, hypertension, and smoking status. Measures in patients with SSD are shown in red and measures in HC, in gray.

Abbreviations: b/a ratio, quotient of the b and a-wave amplitudes; HC, healthy control individuals, N, number of participants; n, number of eyes; q, false discovery rate-adjusted p value; SSD, individuals with schizophrenia spectrum disorders

Tables

Table 1. Cohort characteristics

	SSD		HC		
Demographic characteristics	*Mean* ± *SD*	*N*	*Mean* ± *SD*	*N*	*p*
Age, years	39.08 ± 10.48	103	33.58 ± 11.85	130	**<0.001**[b]
	N (%)		*N* (%)		*p*
Sex, female:male (% female)	34:69 (33%)		65:65 (50%)		**0.011**[a]
Current smoking, yes:no (% yes)	45:54 (45%)		21:109 (16%)		**<0.001**[a]
	Mean ± *SD*	*N*	*Mean* ± *SD*	*N*	*p*
BMI, kg/m^2	29.37 ± 6.50	102	23.34 ± 3.26	130	**<0.001**[b]
Comorbidities	*N* (%)		*N* (%)		*p*
Diabetes, yes:no (% yes)	10:93 (10%)		0:130 (0%)		**<0.001**[a]
Hypertension, yes:no (% yes)	33:70 (32%)		16:114 (12%)		**<0.001**[a]
Eye examinations	*Mean* ± *SD*	*n* (eyes)	*Mean* ± *SD*	*n* (eyes)	*p*
BCVA	1.13 ± 0.19	199	1.12 ± 0.21	257	0.396[b]
IOP, mmHg	13.74 ± 2.59	200	13.26 ± 2.69	258	0.055[c]
Spherical equivalent, D	−1.48 ± 1.64	200	−0.92 ± 1.52	258	**<0.001**[b]
Disease characteristics	*Mean* ± *SD*	*N*	*Mean* ± *SD*	*N*	*p*
Duration of illness, years	13.23 ± 8.75	99	−	−	−
Duration of untreated psychosis, months	24.11 ± 37.39	49	−	−	−
PANSS positive symptoms	11.67 ± 4.26	103	−	−	−
PANSS negative symptoms	12.16 ± 5.03	103	−	−	−
PANSS general symptoms	25.93 ± 7.47	103	−	−	−
PANSS total score	49.57 ± 14.58	103	−	−	−
BACS composite z-score	−1.40 ± 1.28	94	0 ± 1.00	116	**<0.001**[c]
CPZeq, mg	334.58 ± 282.28	94	−	−	−
	N (%)		*N* (%)		
Remission, yes:no (% yes)	43:60 (42%)		−		−
Diagnosis (*DSM-5*)	*N* (%)		−		−
Schizophrenia	74 (72%)		−		−
Schizoaffective disorder	26 (25%)		−		−

Brief psychotic disorder	3 (3%)	–	–
			–
Available data	*N* (*n*)	*N* (*n*)	
OCT	98 (185)	128 (250)	–
ERG	102 (198)	125 (246)	–
MRI	79	112	–

BACS, Brief Assessment of Cognition in Schizophrenia; BCVA, best corrected visual acuity; BMI, body mass index; CPZeq, chlorpromazine equivalent doses; D, diopter; ERG, electroretinography; HC, healthy controls; IOP, intraocular pressure; MRI, magnetic resonance imaging; *N*, number of participants; *n*, number of eyes; *p*, p value; PANSS, Positive and Negative Syndrome Scale; OCT, optical coherence tomography; *SD*, standard deviation; SSD, schizophrenia spectrum disorder

[a] Fisher's exact test

[b] Mann-Whitney *U* test

[c] Welch's *t* test

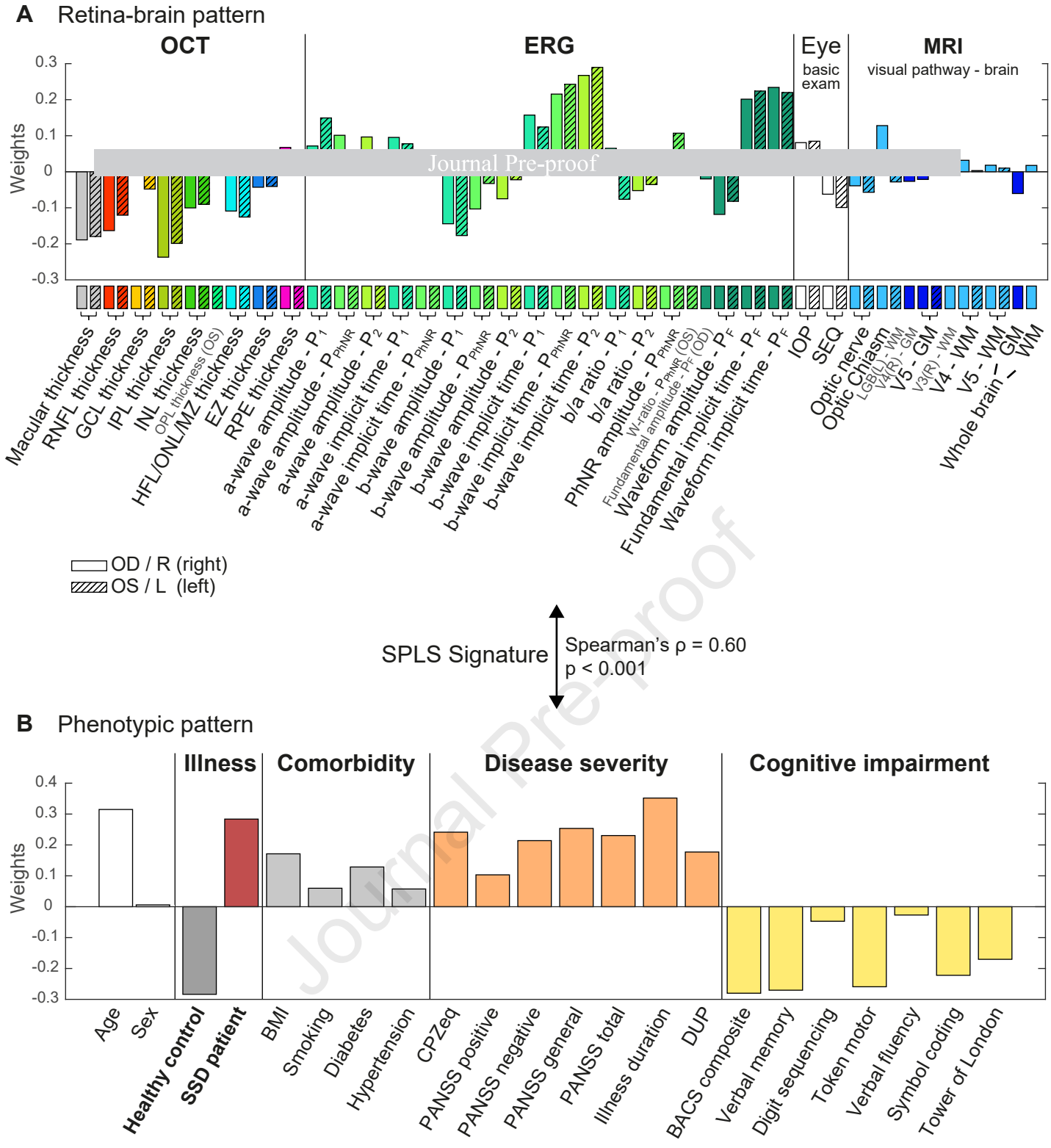
A
Retina-brain pattern
OCT
ERG
Eye
basic exam
MRI
visual pathway - brain
Weights
Journal Pre-proof
Macular thickness
RNFL thickness
GCL thickness
IPL thickness
INL thickness
OPL thickness (OS)
HFL/ONL/MZ thickness
EZ thickness
RPE thickness
a-wave amplitude - P1
a-wave amplitude - PPhNR
a-wave amplitude - P2
a-wave implicit time - P1
a-wave implicit time - PPhNR
b-wave amplitude - P1
b-wave amplitude - PPhNR
b-wave amplitude - P2
b-wave implicit time - P1
b-wave implicit time - PPhNR
b-wave implicit time - P2
b/a ratio - P1
b/a ratio - P2
PhNR amplitude - PPhNR
W-ratio - PPhNR (OS)
Fundamental amplitude - PF (OD)
Waveform amplitude - PF
Fundamental implicit time - PF
Waveform implicit time - PF
IOP
SEQ
Optic nerve
Optic Chiasm
LGB(L) - WM
V4(R) - GM
V5 - GM
V3(R) - WM
V4 - WM
V5 - WM
Whole brain – GM
WM
OD / R (right)
OS / L (left)
SPLS Signature
Spearman's ρ = 0.60
p < 0.001
B
Phenotypic pattern
Illness
Comorbidity
Disease severity
Cognitive impairment
Weights
Age
Sex
Healthy control
SSD patient
BMI
Smoking
Diabetes
Hypertension
CPZeq
PANSS positive
PANSS negative
PANSS general
PANSS total
Illness duration
DUP
BACS composite
Verbal memory
Digit sequencing
Token motor
Verbal fluency
Symbol coding
Tower of London